

## Large electrocaloric response via percolation of polar nanoregions

Xingyue Ma,<sup>1</sup> Yurong Yang <sup>1,\*</sup>, L. Bellaiche,<sup>2</sup> and Di Wu <sup>1,†</sup>

<sup>1</sup>National Laboratory of Solid State Microstructures, Jiangsu Key Laboratory of Artificial Functional Materials, and Department of Materials Science and Engineering, Nanjing University, Nanjing 210093, China

<sup>2</sup>Physics Department and Institute for Nanoscience and Engineering, University of Arkansas, Fayetteville, Arkansas 72701, USA



(Received 19 July 2021; revised 28 January 2022; accepted 1 February 2022; published 14 February 2022)

A first-principle-based effective Hamiltonian model is developed to investigate electrocaloric effects (ECE) of ferroelectric  $\text{Pb}(\text{Sc}_{0.5}\text{Ta}_{0.5})\text{O}_3$  (PST) possessing different degrees of chemical ordering between Sc and Ta cations. It is found that PST exhibits large electrocaloric effects when the electric field drives a paraelectric-to-ferroelectric phase transition isothermally above the Curie temperature. More precisely, for any specific temperature above the Curie temperature, the electrocaloric coefficient exhibits its maximum at a critical electric field that is precisely the threshold of percolation for which the polar nanoregions begin to propagate inside the whole sample, with dipoles being parallel to the field's direction. This percolation-induced maximal ECE occurs for all the possible degrees of chemical ordering, therefore making it a general and novel mechanism, based on which a strategy is further proposed to improve the ECE.

DOI: [10.1103/PhysRevB.105.054104](https://doi.org/10.1103/PhysRevB.105.054104)

### I. INTRODUCTION

The development of highly energy efficient and environmentally friendly refrigeration technologies is of high requirement for the mitigating global warming potential and releasing total greenhouse gas emission. Approximately 20% of the energy consumption in the world is used for refrigeration purposes [1]. The current refrigeration of vapor-compression-cycle-based works with high global warming potential and is environmentally unfriendly. Furthermore, this refrigeration technology is unsuitable for miniaturization in electric cooling application.

The non-vapor-compression-cycle-based cooling technologies have been developed for magnetocalorics, electrocalorics (ECE), and elastocalorics, which undergo large entropy changes driven by magnetic, electric, and mechanical inputs, respectively [2–6]. In comparison with the other caloric effects, ECE regained considerable attention from both academia and industry recently because of their high efficiency, direct electricity utilization, low cost, and mature processes for mass production [6–11].

Among the various investigated ferroelectric, antiferroelectric, and relaxor ECE materials, ferroelectric  $\text{PbSc}_{0.5}\text{Ta}_{0.5}\text{O}_3$  (PST) has received great interest recently, as a large ECE has been observed over a wide temperature range near room temperature [12–14]. More precisely, an adiabatic temperature change ( $\Delta T_S$ ) of about 5.5 K near room temperature was measured for a PST multilayer capacitor (MLC) [12], which was immediately used in cooling devices [13,14]. Surprisingly, the mechanism of this giant ECE in PST is unclear, to the best of our knowledge. Determining it will not only deepen fundamental knowledge of ECE effects but may also be taken

advantage of to further enhance cooling efficiency [15–19]. On the other hand, percolation is a fundamental model in statistical mechanics related to phase transitions signaled by the emergence of a giant connected components. The percolation theory was applied to complex network [20], resistor networks [21], protein interaction network [22], earth's topography and landscapes [23], electrical conductivity [24,25], consumer market [26], stock market [27,28] and social percolation [29]. Percolation models serve as important universality classes in critical phenomena [30].

In this paper, we reveal the microscopic mechanism responsible for the large ECE for temperatures above the Curie temperature in ferroelectric PST being chemically ordered or disordered, by developing and using a first-principle-based effective Hamiltonian approach. The electrocaloric (EC) coefficient, which is defined as the derivative of the temperature with respect to the electric field at constant entropy [ $\alpha = (\frac{\partial T}{\partial E})_S$ ], shows a nonmonotonic behavior with electric field  $E$ , associated with the evolution of polar nanoregions (PNRs) or the development of macroscopic polarization driven by the electric field from paraelectric to ferroelectric states above the Curie temperature. The maximum of  $\alpha$  in the  $\alpha$ -versus- $E$  curve happens for the electric field that induces the percolation of PNRs, which is therefore the microscopic origin of the observed giant ECE above the Curie temperature.

This paper is organized as follows. Section II describes the effective Hamiltonian approach. Sections III A and III B analyze the ECE for perfectly rocksalt ordered PST and partly ordered PST, respectively. Finally, Sec. IV concludes this work.

### II. METHODS

We developed a first-principle-based effective Hamiltonian approach for PST based on the virtual crystal approximation (VCA) [31] for which Sc and Ta ions are replaced by a virtual

\*yangyr@nju.edu.cn

†diwu@nju.edu.cn

average atom  $\langle B \rangle$ . The effective Hamiltonian has two main terms:

$$E_{\text{tot}}(\{\mathbf{u}_i\}, \{\mathbf{v}_i\}, \{\omega_i\}, \{\sigma_i\}, \eta_H) = E_{\text{ave}}(\{\mathbf{u}_i\}, \{\mathbf{v}_i\}, \{\omega_i\}, \eta_H) + E_{\text{loc}}(\{\mathbf{u}_i\}, \{\mathbf{v}_i\}, \{\omega_i\}, \{\sigma_i\}), \quad (1)$$

where  $\{\mathbf{u}_i\}$  is the Pb-centered local soft mode vector at site  $i$ , which is directly proportional to the local electric dipole;  $\{\mathbf{v}_i\}$  is the Pb-centered dimensionless vector, which is related to the inhomogeneous strain at site  $i$ ;  $\{\omega_i\}$  is the B-site-centered pseudovector quantifying the oxygen octahedral tilting at site  $i$ , also commonly called antiferrodistortive (AFD) distortions;  $\{\sigma_i\}$  is the variable describing the chemical configuration, where  $\sigma_i = 1$  or  $-1$  denotes Sc or Ta atom at site  $i$ , respectively, and  $\eta_H$  is the homogeneous strain tensor.

The  $E_{\text{ave}}$  term treats the two types of  $B$ -site atoms as a virtual atom  $\langle B \rangle$ . The analytical form of  $E_{\text{ave}}$  is in the form previously provided for *simple* perovskite compounds such as  $\text{NaNbO}_3$ , and is given in, e.g., Refs. [32–34].

For  $E_{\text{loc}}$ , we use the following expression [35–37]:

$$E_{\text{loc}}(\{\mathbf{u}_i\}, \{\mathbf{v}_i\}, \{\omega_i\}, \{\sigma_i\}) = \sum_{i,j} Q_1 \sigma_j \mathbf{e}_{ji} \cdot \mathbf{u}_i + \sum_{i,j} R_1 \sigma_j \mathbf{f}_{ji} \cdot \mathbf{v}_i + \sum_i \omega_i \left( A_0 \sigma_i + \sum_j A_1 \sigma_j \right), \quad (2)$$

where  $\omega_i = |\omega_i|$ . The sums over  $i$  run over all Pb sites, while the sums over  $j$  run over the eight nearest neighbor  $\langle B \rangle$  sites of the site  $i$ .  $\mathbf{e}_{ji}$  and  $\mathbf{f}_{ji}$  are unit vectors joining the  $B$ -site  $j$  to the Pb-center  $i$ .

The parameters in the effective Hamiltonian are determined by performing first-principle calculations on relatively small cells (up to 30 atoms), using the Vienna *Ab initio* Simulation Package (VASP) and the projected augmented wave (PAW) method [38–40], altogether with the density functional theory (DFT) with local density approximation (LDA) [41]. Following the notations used in Refs. [32,35], the effective Hamiltonian parameters for PST are listed in Table S1 in the Supplemental Materials (SM) [12,42–48].

We performed Monte Carlo (MC) simulations within this effective Hamiltonian on  $12 \times 12 \times 12$  supercells (8640 atoms) with the Metropolis algorithm [49] in the isothermal-isobaric ensemble (NPT ensemble), from which the enthalpy is directly available as

$$H = E_{\text{tot}} + \frac{21}{2} N k_B T + pV - \mathbf{V} \mathbf{E} \cdot \mathbf{P}, \quad (3)$$

where  $E_{\text{tot}}$  is given by Eq. (1),  $p$  is the pressure,  $V$  is the supercell volume,  $\mathbf{E}$  is the electric field,  $\mathbf{P} = \frac{Z^*}{V} \sum_i \mathbf{u}_i$  is the polarization,  $N$  is the number of five-atom unit cells in the supercell and the term  $\frac{21}{2} N k_B T$  contains potential energy of six degrees of freedom and kinetic energy of 15 degrees of freedom in each site, which are not included in  $E_{\text{tot}}$  [48]. Considering the fact that LDA often underestimates the lattice constant, we applied a negative external pressure of  $-6.5$  GPa in our simulations. Typically,  $1 \times 10^6$  MC sweeps are used for equilibration and an additional  $1 \times 10^6$  MC sweeps are used to compute the statistical averages at temperature  $T$  and electric field  $E$  to obtain converged results.

Note that the electric fields here have been rescaled linearly as  $\tilde{E} = cE$ , where  $E$  is original electric field in our MC calculations,  $\tilde{E}$  is rescaled electric field,  $c$  is a constant and is chosen to be 0.2 in this work. This rescaling scheme is inspired from the fact that the electric field is usually overestimated by about one order of magnitude in the atomic effective Hamiltonian schemes (possibly because of the so-called Landauer paradox) [17,46].

We consider PST systems with different ordering degrees, characterized by  $S = |SOF(\text{Sc}) - SOF(\text{Ta})| / |SOF(\text{Sc}) + SOF(\text{Ta})|$  [50], where  $SOF$  is the site occupation factor of the (4a) [or equivalently, (4b)] Wyckoff position in the  $Fm\bar{3}m$  structure. Practically, we constructed alloy configurations with specified  $S \in (0, 1)$  by first constructing a perfect rocksalt-ordered configuration, and then exchanging  $B$ -site cations randomly until  $S$  is equal to the given predefined value. For the fully disordered configurations  $S = 0$ , Sc and Ta ions are distributed randomly. For any partly ordered PST with  $S < 1$ , we perform simulations on different configurations, all with the same specified  $S$  value, and then average the results.

Moreover, the linear EC coefficient  $\alpha$  is the derivative of the temperature with respect to the electric field at constant entropy, which is computed from MC simulations by the following cumulant formula [17,48]

$$\alpha = -Z^* N T \left[ \frac{\langle uH \rangle - \langle u \rangle \langle H \rangle}{\langle H^2 \rangle - \langle H \rangle^2 + \frac{21}{2} (k_B T)^2} \right], \quad (4)$$

where  $Z^*$  is the Born effective charge,  $N$  is the number of the sites in the supercell,  $T$  is the temperature,  $H$  is the enthalpy defined in Eq. (3).  $V$  is the supercell volume,  $\mathbf{E}$  is the external electric field,  $p$  is the external pressure, and  $\langle \cdot \rangle$  defines the average over the MC sweeps at a given temperature. Practically,  $\alpha$  is calculated at a certain temperature and under a *dc* electric field applied along the pseudocubic [111] direction, which is the direction of the spontaneous polarization in PST below the Curie temperature [8,51,52]. The isothermal entropy change ( $\Delta S$ ) and adiabatic temperature change ( $\Delta T_S$ ) on removal of electric field are also computed from MC simulations, see more details in the SM [42].

### III. RESULTS AND DISCUSSION

#### A. Ordered configuration

We first focus on PST with perfectly rocksalt-ordered  $B$ -site atoms, and which has been reported to have giant ECE [9,12]. Figure 1(a) shows the polarization  $P(\tilde{E}, T)$  diagram as functions of temperature  $T$  and electric field  $\tilde{E}$ , as obtained by cooling simulations under electric field applied along the pseudocubic [111] direction [53]. Under high electric field and at low temperature, PST is in the ferroelectric phase [upper left side in red in Fig. 1(a)], while it is in the paraelectric phase under low electric field and high temperature [lower right corner in blue in Fig. 1(a)]. The olivine colored region in-between represents the phase coexistence line or the supercritical phase where the ferroelectric and paraelectric states become indistinguishable. Our calculated critical end point that separates the subcritical (where ferroelectric and paraelectric phases can be distinguished) from the supercritical region, is located at

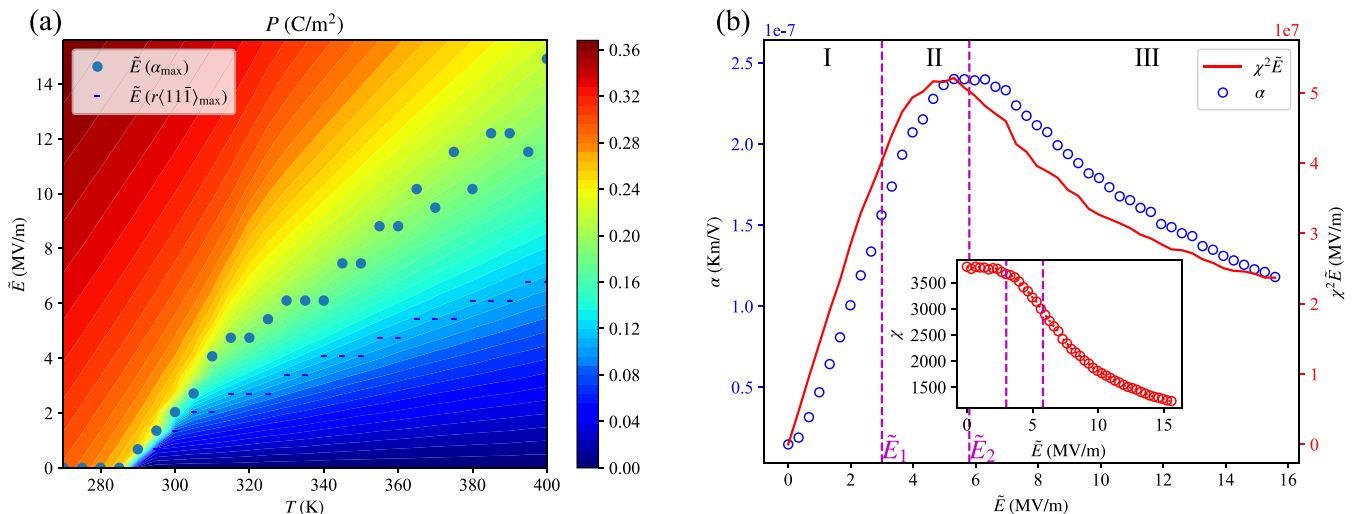


FIG. 1. (a) Polarization  $P(\vec{E}, T)$  as a function of electric field  $\vec{E}$  and temperature  $T$  and (b) EC coefficient  $\alpha$  as a function of electric field at 330 K. The electric field for which  $\alpha$  exhibits its maximum [ $\vec{E}(\alpha_{\max})$ ] and the electric field at which  $r(11\bar{1})$  exhibits its maximum [ $\vec{E}(r(11\bar{1}))$ ] for the investigated temperatures are shown in panel (a).  $\chi^2\vec{E}$  is shown in panel (b) to compare it with  $\alpha$ .

about 3.38 MV/m at 305 K. Note that the ECE is known to be large in the supercritical region [12,43,54]. Furthermore, our calculated  $P(\vec{E}, T)$  diagram is very well consistent with measurements [12]. For instance, at 270 K and 15.59 MV/m, the simulations provide a polarization of 0.376 C/m<sup>2</sup> to be compared with the measured 0.362 C/m<sup>2</sup> value, indicating the accuracy of our numerical method.

Furthermore, Fig. 1(b) displays  $\alpha$  as a function of  $\vec{E}$  at a temperature of 330 K, which is slightly higher than the calculated Curie temperature of 290 K (which coincides with the measured one [12]) and room temperature.  $\chi^2\vec{E}$  is also shown in Fig. 1(b) for comparison, since  $\alpha$  versus  $\vec{E}$  at any temperature above the critical temperature was proposed to satisfy the simple Landau-like model  $\alpha = \beta T \frac{\partial P^2}{\partial \vec{E}} = 2\beta T \epsilon_0^2 \chi^2 \vec{E}$  in relaxors [17,18]. One can see that  $\alpha$  does satisfy this Landau-like model very well (with  $\beta = 0.0890$  m<sup>4</sup>/C<sup>2</sup> here). Moreover, the  $\alpha(\vec{E})$  curve can be divided into three regions, as shown in Fig. 1(b). In the low field region-I below 3.0 MV/m,  $\alpha$  increases sharply and linearly with increasing  $\vec{E}$ , as a result of the large and nearly constant dielectric susceptibility  $\chi$  at low electric field [see inset of Fig. 1(b)]. Under intermediate electric field, region-II with 3.0 MV/m <  $\vec{E}$  < 5.8 MV/m,  $\alpha$  slowly increases with  $\vec{E}$  and reaches its maximum at about 5.8 MV/m. This maximum results from competition between the increase of  $\vec{E}$  and the decrease of  $\chi^2$ . For region-III, where the electric field is larger than 5.8 MV/m, the rapid decrease of  $\chi^2$  with  $\vec{E}$  dominates the  $\alpha$ -versus- $\vec{E}$  behavior and  $\alpha$  begins to decrease with increasing  $\vec{E}$ .

Furthermore, the EC coefficient  $\alpha(T, \vec{E})$  is shown in Fig. 2(a).  $\alpha$  at the phase coexistence line and within the supercritical phase shown in the  $P(\vec{E}, T)$  diagram [see Fig. 1(a)] is much larger than that in the ferroelectric and paraelectric phases. One can clearly see that, for a certain temperature above the Curie temperature of about 290 K [see also Fig. 1(b)],  $\alpha$  exhibits a nonmonotonic behavior with electric field, consisting of an increase up to a maximum ( $\alpha_{\max}$ ) from

a small value at zero field, followed by a decrease at higher fields. The electric fields  $\vec{E}(\alpha_{\max})$ , at which  $\alpha_{\max}$  occurs, for specific temperatures are shown in Fig. 1(a).  $\vec{E}(\alpha_{\max})$  coincides with the phase coexistence line and the supercritical phase. The broad supercritical phase region at higher electric field [olivine in the  $P(\vec{E}, T)$  diagram] also implies that giant electrocaloric response occurs over a wide temperature range.

To understand the large EC response in PST at a local scale, we decided to analyze the dipolar configuration by percolation theory [55,56].

Two specific quantities are computed from our MC simulations. The first one is the so-called percolation strength, which is calculated as  $P_\infty = \frac{N_\infty}{N_{\text{Pb}}}$ , where  $N_\infty$  is the number of distinct Pb sites within the percolating clusters, and  $N_{\text{Pb}}$  is the total number of Pb sites in the supercell [18,44]. Note that the percolating clusters are defined as the PNRs that spread from one side to another side in the supercell, and which thus have an infinite size under periodic boundary conditions. The PNRs are practically determined by comparing directions of dipoles with their nearest neighbors, as in Ref. [57]. The second quantity is the average cluster size defined as  $\langle s \rangle = \langle N_p^2 \rangle / \langle N_p \rangle$ , where  $N_p$  is the number of local dipoles within a PNR and where  $\langle \cdot \rangle$  denotes average over all PNRs [18,56].

Figure 3(a) shows  $P_\infty$  as a function of temperature and electric field. One can clearly see that, for any reported temperature, the electric field exhibiting the maximal change of  $P_\infty$  ( $\vec{E}[(\Delta P_\infty)_{\max}]$ ) (i.e., the electric field for which  $\frac{dP_\infty(\vec{E})}{d\vec{E}}$  is maximum) coincides well with the field inducing the maximal EC coefficient  $\alpha_{\max}$ . On the other hand, the maximum of  $r(11\bar{1})$  (which is defined as the percentage of local dipoles lying near  $[11\bar{1}]$ ,  $[1\bar{1}1]$ , or  $[\bar{1}11]$  pseudocubic directions, i.e., the  $\langle 111 \rangle$  directions that have a positive projection on the direction of  $\vec{E}$  except the  $[111]$  field's direction) with respect to electric field is much lower than that of  $\alpha_{\max}$  and  $(\Delta P_\infty)_{\max}$  for any investigated temperature. This contrasts from the relaxor Pb(Mg,Nb)O<sub>3</sub> (PMN), for which  $r(11\bar{1})$  exhibits its

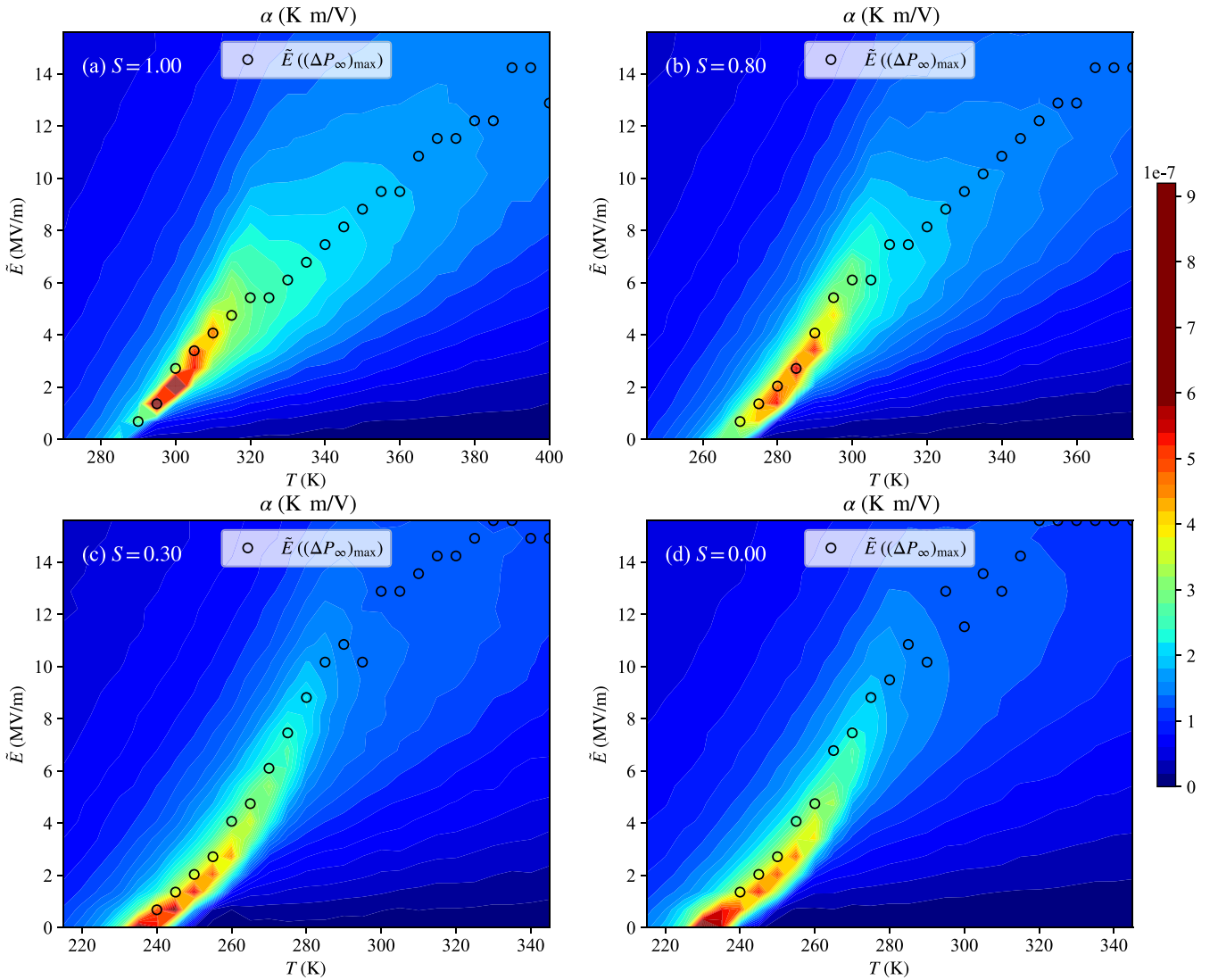


FIG. 2. EC coefficient  $\alpha(T, \tilde{E})$  as a function of electric field and temperature for PST with various degrees of chemical ordering (a)  $S = 1.0$ , (b)  $S = 0.8$ , (c)  $S = 0.3$ , and (d)  $S = 0.0$ . The electric field  $(\Delta P_\infty)_{\max}$  for considered temperature is shown by open circles.

maximum at the same electric field with  $\alpha_{\max}$  [18]. Figure 3(b) displays the strength of the percolating cluster  $P_\infty(\tilde{E})$  at 330 K. Similar to Fig. 1(b), the whole field range can be split into three regions. In region-I where  $\tilde{E}$  is small,  $P_\infty$  vanishes and the cluster size increases slowly from about 3 to 5 with increasing  $\tilde{E}$ . This is again different from PMN relaxors [18], where the PNR size remains constant in the small field region. This may be ascribed to the rather large dielectric susceptibility  $\chi$  [see Fig. 1(b)] in ferroelectric PST near the Curie temperature, as compared with that of PMN relaxors near its critical point, where a first-order transition becomes a second-order one [18]. In field region-II with intermediate  $\tilde{E}$ ,  $P_\infty$  starts to increase slowly with a sharp increase of cluster size  $\langle s \rangle$  [shown in the right inset of Fig. 3(b)]. Note that the maximum of  $r(11\bar{1})$  occurs at 3.4 MV/m, that is in region-II. With  $\tilde{E}$  further increasing into region-III,  $P_\infty$  increases significantly at the beginning of such region but then increases slower at large electric field in this region-III. In fact, the  $P_\infty$  in region-III can be well fitted by a  $(\tilde{E} - \tilde{E}_2)^\beta$  power law [56] with the threshold of percolation  $\tilde{E}_2$  being equal to

5.8 MV/m and  $\beta = 0.36$  for the chosen temperature of 330 K. The value of  $\tilde{E}_2$  is very close to the electric field associated with  $(\Delta P_\infty)_{\max}$ , for which the EC coefficient also exhibit their maximum. We also investigated percolation at higher temperatures, and found that the optimal EC coefficient  $\alpha_{\max}$  occurs at the electric field close to the  $\tilde{E}_2$  for all the investigated temperatures, with  $\tilde{E}_2$  depending on temperature. Similarly, the maximum of  $r(11\bar{1})$  with respect to field is found to occur at a field smaller than the threshold field of percolation for any studied temperature above the Curie temperature. It is therefore the percolation of PNRs, rather than the change of dipole directions, that induces the large ECE in PST.

Figure 4 shows the microscopic dipole configurations under electric field with different magnitudes, at 330 K. As shown in Figs. 4(a) and 4(b), the largest size of PNR at 1.66 MV/m is only slightly larger than that for zero field. This is consistent with the  $\langle s \rangle(\tilde{E})$  curve shown in Fig. 3(b) where  $\langle s \rangle$  slowly increases at low field. As  $\tilde{E}$  increases within region-II,  $\langle s \rangle$  increases quickly with increasing  $\tilde{E}$  [see Figs. 4(c) and 4(d)]. Note that  $r(11\bar{1})$  reaches its maximum (see Fig. S3

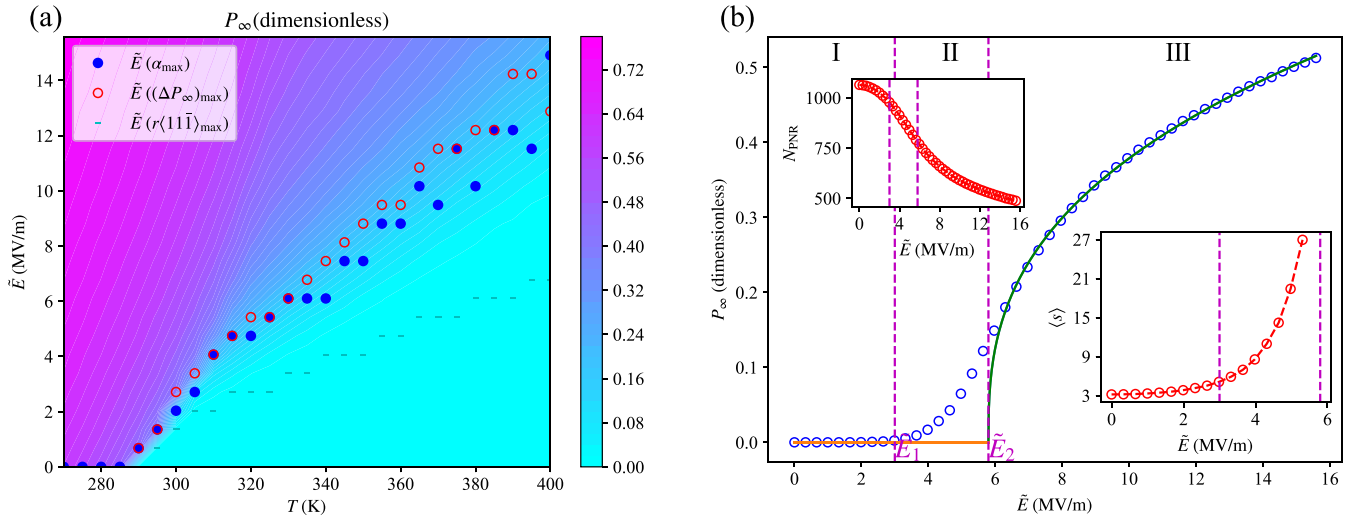


FIG. 3. Percolation strength  $P_\infty$  (a) at any investigated temperature and electric field and (b) as a function of electric field at the temperature of 330 K. The electric fields associated with  $\alpha_{\max}$ ,  $\Delta P_{\infty, \max}$ , and  $r\langle 11\bar{1}\rangle_{\max}$  are shown in panel (a) for any investigated temperature. The left inset of panel (b) shows the number of PNRs ( $N_{\text{PNR}}$ ) as a function of electric field at 330 K. The right inset of panel (b) shows the average cluster size  $\langle s \rangle$  as a function of electric field at 330 K. The green curve represents the fitting of the power law (see text) while the horizontal orange lines are guides for the eye.

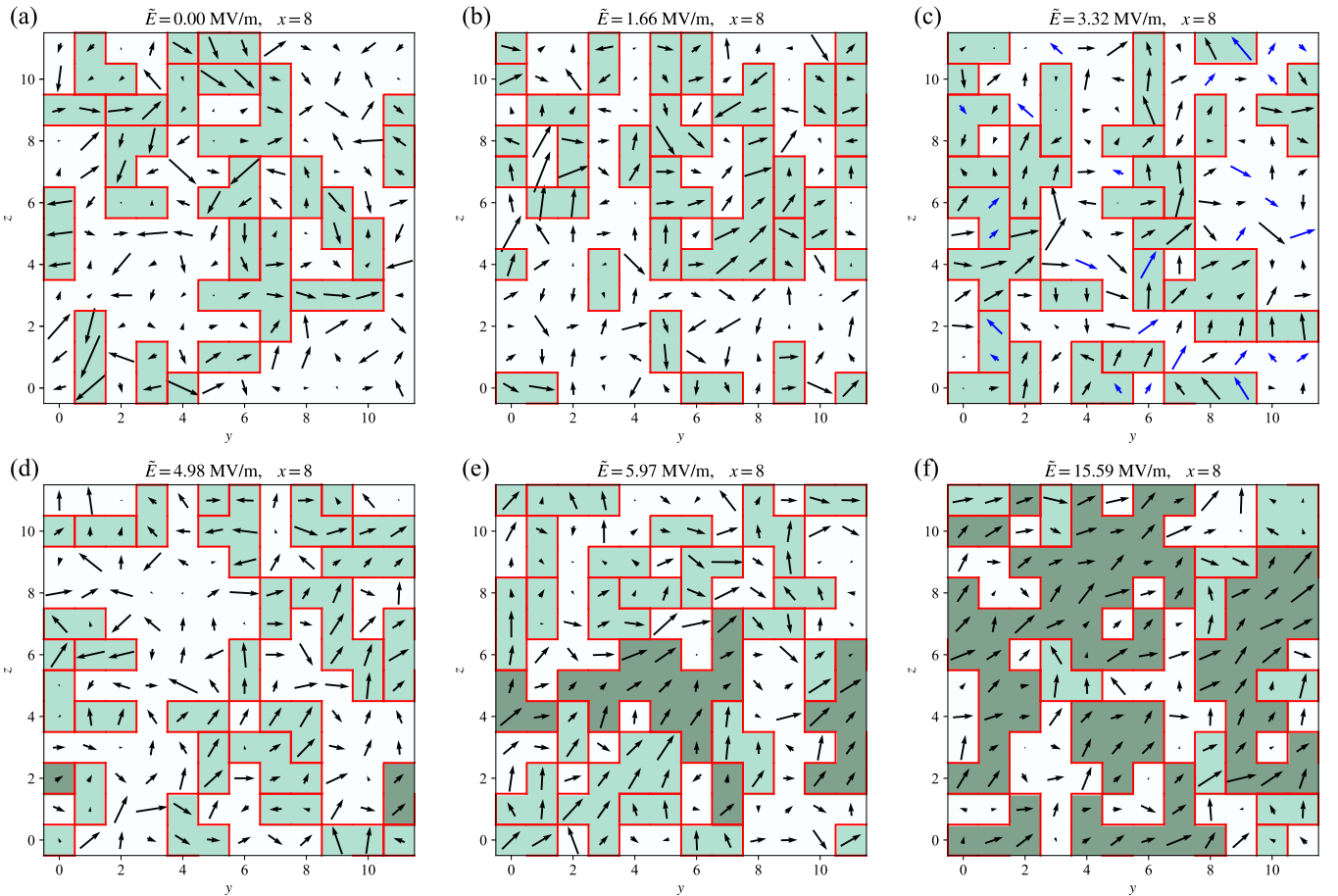


FIG. 4. Snapshots of dipolar configurations in a given  $(x, y)$  plane (for which  $x = 8$ ) for different electric fields applied along the  $[111]$  direction in perfectly rocksalt-ordered PST at 330 K. Panels (a), (b), (c), (d), (e), and (f) correspond to the electric field at 0, 1.66 (region-I), 3.32 (maximum of  $r\langle 11\bar{1}\rangle$ ), 4.98 (region-II), 5.97 ( $\alpha_{\max}$ ), and 15.59 MV/m (region-III), respectively. Arrows indicate the local modes, blue arrows in panel (c) indicate the corresponding dipoles lying near  $\langle 11\bar{1}\rangle$ ,  $\langle \bar{1}11\rangle$ , or  $\langle 111\rangle$ , which contribute to  $r\langle 11\bar{1}\rangle$ . Solid red lines are used to delimit PNRs. White, light green, and deep green colored regions are used to differentiate non-PNRs, PNRs, and percolating PNRs, respectively.

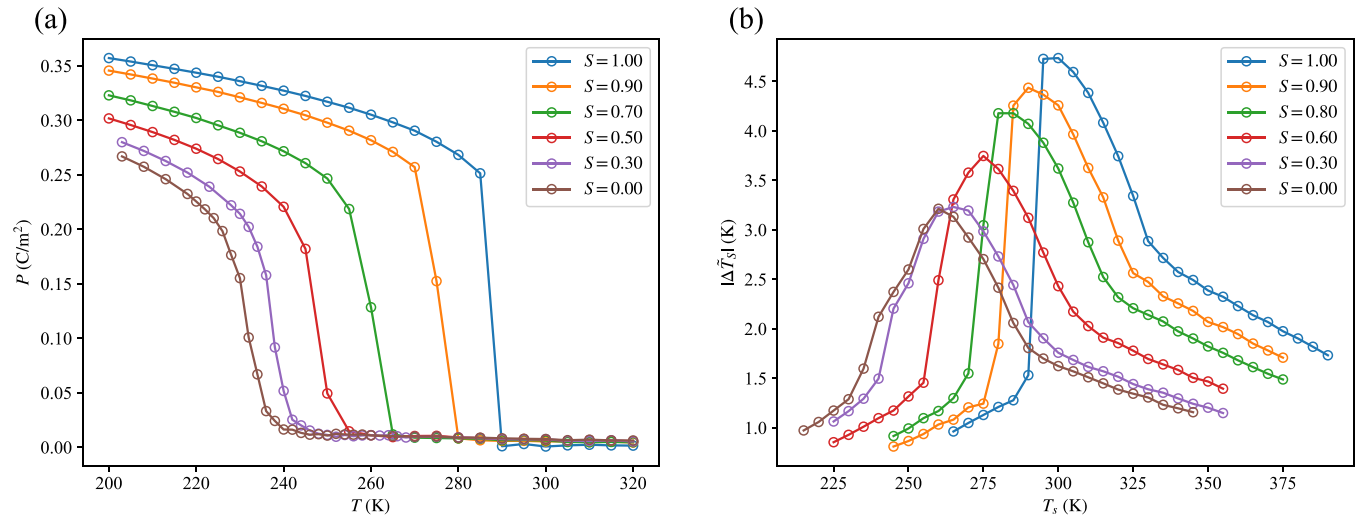


FIG. 5. (a) Polarization  $P$  of PST with various degrees of chemical ordering  $S$  as a function of temperature. (b) The adiabatic temperature change  $|\Delta \tilde{T}_S|$  of PST with various degrees of chemical ordering  $S$  due to the removal of the electric field  $\vec{E} = 15.59$  MV/m from each considered temperature.

in the SM [42]) at 3.32 MV/m in region-II, implying the easy rotation of dipoles for this field. When  $\vec{E}$  increases to 5.97 MV/m in the region-III, very close to  $\vec{E}_2$ , relatively large percolating clusters can be seen in Fig. 4(e). Near this field, the gradient of  $P_\infty$  with respect to  $\vec{E}$  exhibits a maximum [see Fig. 3(b)], indicating the fast formation of percolating clusters and the long-range ferroelectric interaction penetrates through the whole sample, which reduces the entropy greatly and therefore leads to large ECE.

Further increasing the field,  $P_\infty$  increases and large percolation region forms. Please note that the spatial position of percolating clusters can change under different electric fields. For example, the percolation in Figs. 4(d), 4(e), and 4(f) occurs at different sites, implying that the percolation process is dynamic in nature.

### B. Partly ordered configurations

We then studied PST with Sc and Ta cations being partly ordered on the perovskite  $B$  sites. Figure 5(a) displays the spontaneous polarization  $P$  as a function of temperature  $T$ . PST systems, with various  $B$ -site cation chemical order degrees  $S = 0, 0.3, 0.5, 0.7, 0.9$ , and 1.0, all exhibit a paraelectric to ferroelectric phase transition. The ferroelectric phase at low temperature is in a rhombohedral structure with a polarization being along the pseudocubic (111) direction and having out-of-phase oxygen octahedra tilting within the  $a^-a^-a^-$  pattern (Glazer's notation [58]). Both the transition temperature  $T_C$  and the polarization at low temperature decrease with the decrease of  $S$ , with the  $T_C$  range of 290–240 K and polarization range of 25–35  $\mu\text{C}/\text{cm}^2$  for different ordering degree being well consistent with measurements [8]. In completely ordered PST with  $S = 1$ ,  $P$  exhibits a sharp transition at  $T_C$ , which is characteristic of a first-order paraelectric-to-ferroelectric phase transition. With the decrease of  $S$ , the phase transition near  $T_C$  becomes more and more diffuse in PST, as demonstrated by the smaller slope around  $T_C$  in the  $P(T)$  curve. This is also consistent with

measurements [8,9]. This diffuse transition can be ascribed to the disorder-induced random electric field that weakens the long-range dipole-dipole interactions [18,59]. Note that this random field is quantitatively described by the term  $E_{\text{loc}}$  in our effective Hamiltonian model, as shown in Eqs. (1) and (2).

The effects of ordering degree on the polarization and Curie temperature influence the electrocaloric response. As a matter of fact and as shown in Fig. 5(b), the maximum of adiabatic temperature change ( $|\Delta T_S|$ ) under 15.59 MV/m decreases as the ordering degree reduces (note that the predicted maximum of  $|\Delta T_S|$  for completely ordered configuration ( $S = 1$ ) is about 4.73 K, which is consistent with the value of 4.8 K obtained in the measurement of Ref. [12]). Furthermore, the temperature range with large EC effects (large  $|\Delta T_S|$ ) varies and can be very wide for different  $S$ . For instance, a  $|\Delta T_S| > 2$  K (respectively, 3 K) can be reached for the temperature range of 235–375 K (respectively, 255–330 K), under an electric field of 15.59 MV/m. Therefore, controlling the ordering degree of ferroelectric alloys, such as PST, becomes an effective way to tune the Curie temperature but also the temperature range of large ECE.

The EC coefficient  $\alpha(T, \vec{E})$  for various  $S$  degree are shown in Fig. 2, along with the fields associated with the maximal change of percolation strength  $P_\infty$ . It can be seen that the temperature range exhibiting large  $\alpha$  (red color in Fig. 2) is different for different  $S$ , which explains the change in  $|\Delta T_S|$  and in the temperature associated with  $\alpha_{\text{max}}$  when varying  $S$ . Interestingly, the critical-like point, exhibiting the maximum  $\alpha$ , occurs at nearly identical  $\vec{E}$  in PST with different  $S$ . Note also that the coincidence of  $\alpha_{\text{max}}$  and  $(\Delta P_\infty)_{\text{max}}$  is satisfied in all investigated ordering degree  $S$  (see Fig. 2), implying that the EC response of ferroelectric materials with different polarization and  $T_C$  can be well analyzed and understood within the proposed PNR percolation scenario. Furthermore, we performed additional calculations on superlattices made by PST and virtual materials with stronger ferroelectricity [42]. We found these superlattices produce larger  $\Delta \tilde{T}_S$  and lower  $\vec{E}$  required for optimal ECE [42], which further validates the

percolation scenario here and provides a way of enhancing ECE in ferroelectric materials.

It is also interesting to notice that the percolation mechanism revealed here is *not* generally valid for PMN. As a matter of fact and in contrast with the present case,  $E[(\Delta P_{\infty})_{\max}]$  is much larger than  $E(\alpha_{\max})$  for temperatures above the critical point in PMN, according to Ref. [18]. The difference between PMN and PST may arise from the fact that the so-called random electric field [59] is stronger in PMN than in PST (as a result of the facts that Mg belongs to column II of the Periodic Table while Sc belongs to column III, and that both Nb and Ta belong to column V), as evidenced by the nonpolar ground state of PMN as compared to the ferroelectric ground state of PST. Therefore, the long-range order between local dipoles in PMN is broken by this strong random electric field, making percolating clusters harder to form there. Consequently, the percolation of dipoles in PMN is relatively restrained and cannot be the dominating mechanism of ECE in PMN.

#### IV. SUMMARY

In summary, we developed a first-principle-based effective Hamiltonian model, which allows to investigate the finite-temperature physical properties, including EC response, in

PST with different chemical ordering degrees. Our results not only reproduce experimental results for rocksalt-ordered PST [8,12], but also reveal that the field-induced percolation of polar nanoregions is the driving mechanism for inducing large EC coefficient for any degree of *B*-site ordering. We thus hope that our study not only leads to a better understanding of ECE in ferroelectrics, but will also encourage investigations using percolation to enhance electrocaloric conversion and to design novel electrocaloric materials.

#### ACKNOWLEDGMENTS

We thank the useful discussions with Professor Bin Xu. X.M., Y.Y., and D.W. thank the National Key R&D Program of China (Grant No. 2020YFA0711504), the National Science Foundation of China (Grants No. 11874207, No. 51725203, No. 51721001, No. 52003117, and No. U1932115) and the Natural Science Foundation of Jiangsu Province (Grant No. BK20200262). L.B. acknowledges the Office of Naval Research for the support under Grant No. N00014-21-1-2086 and the Vannevar Bush Faculty Fellowship Grant No. N00014-20-1-2834 from the Department of Defense. We are grateful to the HPCC resources of Nanjing University for the calculations.

- 
- [1] IEA, The Future of Cooling, Tech. Rep. (IEA, Paris, 2018).
  - [2] S. Fähler, U. K. Röbler, O. Kastner, J. Eckert, G. Eggeler, H. Emmerich, P. Entel, S. Müller, E. Quandt, and K. Albe, *Adv. Eng. Mater.* **14**, 10 (2012).
  - [3] L. Mañosa, A. Planes, and M. Acet, *J. Mater. Chem. A* **1**, 4925 (2013).
  - [4] X. Moya, S. Kar-Narayan, and N. D. Mathur, *Nat. Mater.* **13**, 439 (2014).
  - [5] I. Takeuchi and K. Sandeman, *Phys. Today* **68**(12), 48 (2015).
  - [6] X. Moya and N. D. Mathur, *Science* **370**, 797 (2020).
  - [7] Y. V. Sinyavsky, N. D. Pashkov, Y. M. Gorovoy, G. E. Lugansky, and L. Shebanov, *Ferroelectrics* **90**, 213 (1989).
  - [8] N. Setter and L. E. Cross, *J. Appl. Phys.* **51**, 4356 (1980).
  - [9] C. G. F. Stenger and A. J. Burggraaf, *Phys. Status Solidi A* **61**, 653 (1980).
  - [10] P. Kobeko and J. Kurtschatov, *Z. Phys.* **66**, 192 (1930).
  - [11] J. Shi, D. Han, Z. Li, L. Yang, S.-G. Lu, Z. Zhong, J. Chen, Q. Zhang, and X. Qian, *Joule* **3**, 1200 (2019).
  - [12] B. Nair, T. Usui, S. Crossley, S. Kurdi, G. G. Guzmán-Verri, X. Moya, S. Hirose, and N. D. Mathur, *Nature (London)* **575**, 468 (2019).
  - [13] A. Torelló, P. Lheritier, T. Usui, Y. Nouchokgwe, M. Gérard, O. Bouton, S. Hirose, and E. Defay, *Science* **370**, 125 (2020).
  - [14] Y. Wang, Z. Zhang, T. Usui, M. Benedict, S. Hirose, J. Lee, J. Kalb, and D. Schwartz, *Science* **370**, 129 (2020).
  - [15] M. C. Rose and R. E. Cohen, *Phys. Rev. Lett.* **109**, 187604 (2012).
  - [16] R. Pirc, Z. Kutnjak, R. Blinc, and Q. M. Zhang, *J. Appl. Phys.* **110**, 074113 (2011).
  - [17] Z. Jiang, S. Prokhorenko, S. Prosandeev, Y. Nahas, D. Wang, J. Íñiguez, E. Defay, and L. Bellaiche, *Phys. Rev. B* **96**, 014114 (2017).
  - [18] Z. Jiang, Y. Nahas, S. Prokhorenko, S. Prosandeev, D. Wang, J. Íñiguez, and L. Bellaiche, *Phys. Rev. B* **97**, 104110 (2018).
  - [19] I. Ponomareva and S. Lisenkov, *Phys. Rev. Lett.* **108**, 167604 (2012).
  - [20] J. Nagler, A. Levina, and M. Timme, *Nat. Phys.* **7**, 265 (2011).
  - [21] D. C. Wright, D. J. Bergman, and Y. Kantor, *Phys. Rev. B* **33**, 396 (1986).
  - [22] J. Kim, P. L. Krapivsky, B. Kahng, and S. Redner, *Phys. Rev. E* **66**, 055101(R) (2002).
  - [23] A. A. Saberi, *Phys. Rep.* **578**, 1 (2015).
  - [24] C. C. Chen and Y. C. Chou, *Phys. Rev. Lett.* **54**, 2529 (1985).
  - [25] S. Kirkpatrick, *Rev. Mod. Phys.* **45**, 574 (1973).
  - [26] J. Goldenberg, B. Libai, S. Solomon, N. Jan, and D. Stauffer, *Physica A* **284**, 335 (2000).
  - [27] D. Stauffer and T. Penna, *Physica A* **256**, 284 (1998).
  - [28] D. Stauffer and D. Sornette, *Physica A* **271**, 496 (1999).
  - [29] S. Solomon, G. Weisbuch, L. de Arcangelis, N. Jan, and D. Stauffer, *Physica A* **277**, 239 (2000).
  - [30] J. L. Cardy, *J. Phys. A: Math. Theor.* **25**, L201 (1992).
  - [31] L. Bellaiche and D. Vanderbilt, *Phys. Rev. B* **61**, 7877 (2000).
  - [32] Y. Yang, B. Xu, C. Xu, W. Ren, and L. Bellaiche, *Phys. Rev. B* **97**, 174106 (2018).
  - [33] L. Chen, B. Xu, Y. Yang, and L. Bellaiche, *Adv. Funct. Mater.* **30**, 1909496 (2020).
  - [34] W. Zhong, D. Vanderbilt, and K. M. Rabe, *Phys. Rev. B* **52**, 6301 (1995).
  - [35] I. A. Kornev, L. Bellaiche, P.-E. Janolin, B. Dkhil, and E. Suard, *Phys. Rev. Lett.* **97**, 157601 (2006).
  - [36] A. Al-Barakaty, S. Prosandeev, D. Wang, B. Dkhil, and L. Bellaiche, *Phys. Rev. B* **91**, 214117 (2015).
  - [37] L. Bellaiche, A. García, and D. Vanderbilt, *Phys. Rev. Lett.* **84**, 5427 (2000).

- [38] G. Kresse and J. Furthmüller, *Comput. Mater. Sci.* **6**, 15 (1996).
- [39] P. E. Blöchl, *Phys. Rev. B* **50**, 17953 (1994).
- [40] G. Kresse and D. Joubert, *Phys. Rev. B* **59**, 1758 (1999).
- [41] R. O. Jones and O. Gunnarsson, *Rev. Mod. Phys.* **61**, 689 (1989).
- [42] See Supplemental Material at <http://link.aps.org/supplemental/10.1103/PhysRevB.105.054104> for more information about (i) the parameters of effective Hamiltonian used here, (ii) the numerical scheme of the indirect EC calculation, (iii) more properties at 330 K and 360 K, (iv) some of the results of indirect EC calculation for nonordered configurations, and (v) the additional calculations on superlattices that improves ECE.
- [43] M. Otoničar and B. Dkhil, *Nat. Mater.* **19**, 9 (2020).
- [44] A. R. Akbarzadeh, S. Prosandeev, E. J. Walter, A. Al-Barakaty, and L. Bellaiche, *Phys. Rev. Lett.* **108**, 257601 (2012).
- [45] M. Schatzman, *Numerical Analysis : A Mathematical Introduction* (Clarendon Press, Oxford, 2002).
- [46] B. Xu, J. I. Niguez, and L. Bellaiche, *Nat. Commun.* **8**, 15682 (2017).
- [47] S. Bin-Omran, I. A. Kornev, and L. Bellaiche, *Phys. Rev. B* **93**, 014104 (2016).
- [48] Z. Jiang, B. Xu, S. Prosandeev, Y. Nahas, S. Prokhorenko, J. Íñiguez, and L. Bellaiche, *Phys. Rev. B* **103**, L100102 (2021).
- [49] N. Metropolis, A. W. Rosenbluth, M. N. Rosenbluth, A. H. Teller, and E. Teller, *J. Chem. Phys.* **21**, 1087 (1953).
- [50] B. J. Maier, N. Waesermann, B. Mihailova, R. J. Angel, C. Ederer, C. Paulmann, M. Gospodinov, A. Friedrich, and U. Bismayer, *Phys. Rev. B* **84**, 174104 (2011).
- [51] P. M. Woodward and K. Z. Baba-Kishi, *J. Appl. Cryst.* **35**, 233 (2002).
- [52] J. J. P. Peters, A. M. Sanchez, D. Walker, R. Whatmore, and R. Beanland, *Adv. Mater.* **31**, 1806498 (2019).
- [53] The figure is calculated from performing 24 *independent* cooling simulations in parallel, each with a different magnitude of electric field (all along the pseudocubic [111] direction).
- [54] Z. Kutnjak, J. Petzelt, and R. Blinc, *Nature (London)* **441**, 956 (2006).
- [55] D. Stauffre and A. Aharony, *Introduction to Percolation Theory* (Taylor & Francis, New York, 1994).
- [56] S. Prosandeev, D. Wang, A. R. Akbarzadeh, B. Dkhil, and L. Bellaiche, *Phys. Rev. Lett.* **110**, 207601 (2013).
- [57] S. Prosandeev, D. Wang, and L. Bellaiche, *Phys. Rev. Lett.* **111**, 247602 (2013).
- [58] A. M. Glazer, *Acta Cryst. B* **28**, 3384 (1972).
- [59] J. Íñiguez and L. Bellaiche, *Phys. Rev. B* **73**, 144109 (2006).